Eur. Phys. J. D (2013) 67: 63
DOI: 10.1140/epjd/e2013-30547-2

THE EUROPEAN PHYSICAL JOURNAL D

Regular Article

# Ab initio and anion photoelectron studies of $Rh_n$ ($n = 1-9$) clusters*

Marcela R. Beltrán[1,a], Fernando Buendía Zamudio[1], Vikas Chauhan[2], Prasenjit Sen[2], Haopeng Wang[3], Yeon Jae Ko[3], and Kit Bowen[3]

[1] Instituto de Investigaciones en Materiales, Universidad Nacional Autónoma de México, Apartado Postal 70-360, 04510 México D.F., México
[2] Harish-Chandra Research Institute, Chhatnag Road, Jhunsi, 211019 Allahabad, India
[3] Department of Chemistry, Johns Hopkins University, Baltimore, MD 21218, USA

Received 31 August 2012 / Received in final form 19 January 2013
Published online 21 March 2013 – 

**Abstract.** Anion photoelectron spectroscopy (PES) and ab initio calculations have been used to identify the unique structural, electronic, and magnetic properties of both neutral and anionic $Rh_n$ ($n = 1-9$) free standing clusters. Negative ion photoelectron spectra are presented for electron binding energies up to 3.493 eV. We discuss our computational results in the context of the PES experiment, in which the calculated electron affinities and vertical detachment energies are in good agreement with the measured values. Theoretically, we investigate the low-lying energy structures and the spin isomers of each neutral and anionic rhodium cluster and infer their magnetic moments. Our results show that octahedral and tetrahedral motifs are favoured in contrast to cubic motifs. Both experimental and theoretical results obtained here are compared and discussed with previous experimental and theoretical studies on the same systems.

## 1 Introduction

Transition metal (TM) clusters are interesting due to their catalytic as well as their magnetic properties, which are useful for various scientific and technological applications. The magnetic properties of clusters of 3*d* TM atoms, specifically those of the magnetic elements Fe, Co and Ni, have been extensively studied [1–10]. Interesting properties, such as non-monotonic variation of magnetic moments with size were observed in atomic clusters of these elements containing up to a few hundred atoms. These clusters have magnetic moments larger than the corresponding bulk materials. 4*d* transition metals are even more interesting because they are magnetic at the nanoscale while being non-magnetic in the bulk. Not surprisingly, they have been extensively studied over the last decade both experimentally as well as theoretically [11–26]. For any applications, it is of paramount importance to clearly identify the ground state geometries of these clusters, and thus their physical and chemical properties. For example, to establish their role in the field of catalysis in this size regime, recent joint far-infrared multiple photon dissociation (FIR-MPD) experiments and density functional theory (DFT) studies on the reactivity of CO on $Rh_n$ clusters showed the importance of the precise determination of the geometric structures of the TM clusters [23–26]. Another interesting aspect is their magnetic properties. Experiments show that small rhodium clusters with less than 60 atoms have non-zero magnetic moments [15,16]. The enhancement of magnetism in small clusters can be qualitatively understood as a finite-size effect in the electronic structure, and as a consequence of the reduction of local coordination number. The present study has been motivated by the discrepancies found in the literature between numerous theoretical studies undertaken on these clusters. Different calculations have attributed different ground state structures and spin moments at the same cluster size. In some theoretical work [11,12], a singlet ground state in a tetrahedral structure for $Rh_4$ has been reported as the global minimum, while another theoretical study [17] finds a high-spin ground state in a 'bent rhombus' structure. A third effort [23] found a high-spin ground state but with yet another geometry. $Rh_{13}$ is another interesting case. In one study it has been found to possess a magnetic moment of $\sim$1.6 $\mu_B$ per atom in an icosahedral triangular structure [11,12]. A cage-like ground state structure for $Rh_{13}$ clusters with a magnetic moment of 1.3 $\mu_B$ per atom has been reported in reference [17]. On the other hand, in a Stern-Gerlach experiment, a magnetic moment of $\sim$0.48 $\mu_B$ per atom for $Rh_{13}$ has been reported in reference [15,16]. Differences in the structure predictions can explain the apparent discrepancy between different theoretical and experimental

* ISSPIC 16 – 16th International Symposium on Small Particles and Inorganic Clusters, edited by Kristiaan Temst, Margriet J. Van Bael, Ewald Janssens, H.-G. Boyen and Françoise Remacle.

[a] e-mail: mbeltran@unam.mx

results. Thus, it is fair to state that finding the ground state structure of atomic clusters is crucially important in understanding their magnetic properties. Unfortunately there are no direct experimental probes for structures of clusters containing a few atoms. Combining negative ion photoelectron spectroscopy (PES) experiments with first-principles electronic structure calculations has proven to be an effective way to determine structural, electronic and magnetic properties of such clusters [27]. In a recent work [28], we developed understanding of the properties of bi-metallic Rh-Co clusters using such a complimentary approach. In this work, we apply a similar methodology to study pure $Rh_n$ clusters for up to 9 atoms. The experimental photo electron spectra (PES) of the clusters are complemented by theoretical calculations within the density functional theory (DFT) approach. Combining the two studies we have gained fundamental knowledge of their structural, electronic and magnetic properties. We compare our results with previous theoretical calculations and with a recent study which combines (FIR-MPD) experiments with a DFT study on cationic $Rh_n^+$ clusters [29,30]. Our two main focuses were to identify the ground state structures of these clusters, and thereby to understand their electronic and magnetic properties. With regard to their magnetic properties, we found that the magnetic moment varies non-monotonically with size and that several clusters exhibit energetically close spin multiplets. This paper is organized as follows. The details of the method are described in Sections 2 and 3. The results and discussions are presented in Section 4 and the summary in Section 5.

## 2 Experimental methods

Negative ion photoelectron spectroscopy is conducted by crossing a beam of mass selected anions with a fixed-frequency photon beam and energy analyzing the resultant photo-detached electrons. The photo-detachment process is governed by the energy conserving relationship, $h\nu = \mathrm{EBE} + \mathrm{EKE}$, where $h\nu$ is the photon energy, EBE is the electron binding energy, and EKE is the electron kinetic energy. Our apparatus has been described previously elsewhere [31,32]. Briefly, the apparatus consists of an ion source, a linear time-of-flight (TOF) mass spectrometer, a photo-detachment laser, and a magnetic bottle photoelectron spectrometer (MB-PES). The instrumental resolution of the MB-PES is ∼35 meV at 1 eV EKE. The third harmonic (355 nm, 3.493 eV) of a Nd:YAG laser was used to photo-detach the cluster anions of interest. Photoelectron spectra were calibrated as in references [31,32] against the well known atomic transitions of $Cu^-$. In the current study, rhodium cluster anions were generated in a laser vaporization disk source. A rhodium disk was prepared by pressing rhodium powder under a pressure of ∼170 MPa. The disk was ablated by a pulsed Nd:YAG laser beam of 532 nm photons. The plasma was cooled by supersonically expanding a plume of helium carrier gas issued from a general pulsed valve with a backing pressure of ∼1 MPa. The negatively charged clusters were then extracted into our spectrometer for photoelectron spectroscopy studies.

## 3 Computational methods

A density functional theory (DFT) methodology has been used with a TZVP basis set and the ECP28MWB quasi-relativistic ECP core potential [33–36] (the nomenclature for these ECPs is as follows: the number stands for the number of core electrons represented by the ECP; the $M$ stands for the use of the neutral atom in the derivation of the ECP; WB stands for the use of the quasi-relativisitic approach of Wood and Boring [33–36]). The exchange-correlation energy is calculated using the B3LYP hybrid functional which considers a 20% Hartree-Fock exchange [37]. This gives a binding energy ($E_b$, defined later) and bond length of 0.8 eV per atom and 2.27 Å, respectively for the $Rh_2$ dimer. There are very few combinations of exchange-correlation functional and ECP-basis sets that produce both these quantities accurately (see for example Tab. 1 in Ref. [12]). We chose this combination as it gives a reasonable experimental values for the $E_b$ of 1.46 eV, and the experimental bond length of 2.28 Å as reported in reference [38]. At each cluster size we considered a number of initial structures. Each of them was relaxed in the redundant internal coordinates until the forces on all the atoms become smaller than a threshold. A number of spin configurations were considered for each of the structures. The optimization of the cluster geometries was performed without any symmetry constraints. This procedure was followed for both the anionic and neutral clusters. Once the ground state structure and spin multiplicity $M$ ($M = 2S + 1$) of the anion were obtained, the energy of the neutral cluster at the anion geometry was calculated with a multiplicity $M \pm 1$. Their energy difference was then compared with the experimental peaks. This is because if the anion has a multiplicity $M$, the neutral cluster at the same geometry will have a multiplicity of one more or one less depending on whether the electron is removed from the minority or the majority spin channel (unless the anion for odd $n$ has a singlet ($M = 1$) ground state). The lower of these two energies was then used to calculate the vertical detachment energy (VDE) as described below. The Gaussian03 [39] code was used for all our calculations. In this work, we calculated only the spin magnetic moment, and neglected spin-orbit coupling (SOC), although SOC is larger in 4$d$ elements compared to 3$d$ elements. Neglect of SOC can be justified by citing the experimental observation [15,16] that Rh clusters show superparamagnetic behaviour down to 93 K.

## 4 Results

### 4.1 Experimental results PES

Results for the anion photoelectron spectra of pure $Rh_n^-$ clusters for $n = 1-9$ are shown in Figure 1. Each one has been recorded at 355 nm photon energy and plotted as a function of EBE. Features in the spectra represent transitions from the ground electronic state of the anion to the ground electronic, and vibrational states of the corresponding neutral. In particular, the EBE value in the

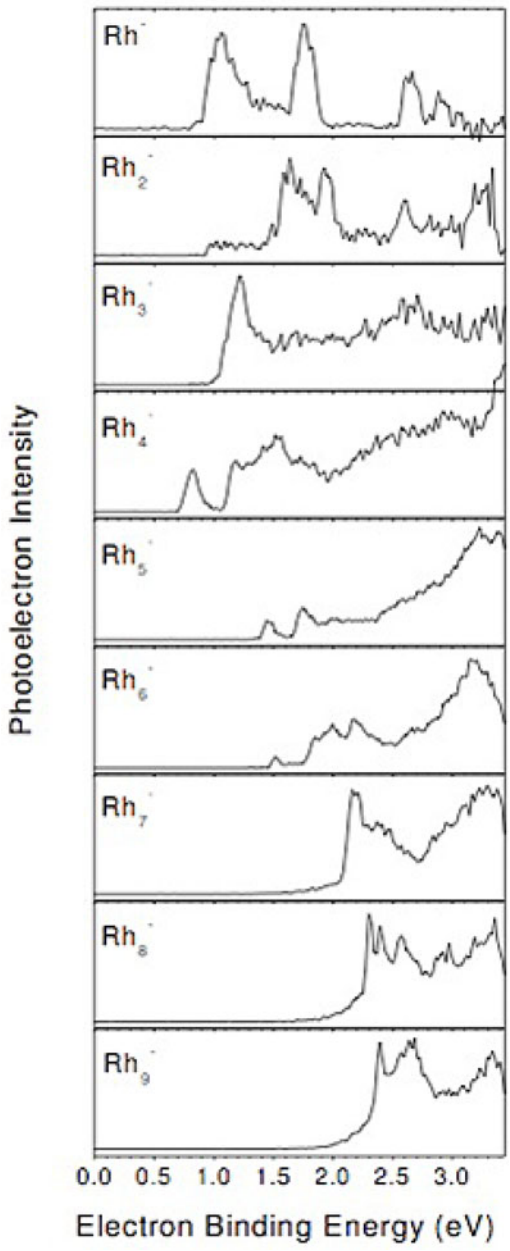


**Fig. 1.** Experimental photoelectron spectra of $Rh_n$ cluster anions for $n = 1-9$.

threshold region of the lowest energy electronic transition, from the ground state of an anion to its corresponding neutral (with the neutral relaxed to its nearest local minimum), is the adiabatic detachment energy (ADE). The ADE is also the adiabatic electron affinity (AEA), when the measured energy difference corresponds to the ground electronic state of both the anion and its neutral species. The EBE peak gives the vertical transition between anion ground state and the neutral cluster at the geometry of the anion, and is defined as the vertical detachment energy (VDE). The experimental ADE and VDE values as obtained from the PES spectra are listed in columns 3 and 4 of Table 1, respectively.

### 4.2 Computational results

The calculated ADE and VDE values of $Rh_n$ clusters ($n = 1-9$) were obtained by means of density functional theory (DFT) calculations. These are listed in columns 5 and 6 in Table 1 and are generally in agreement with the same quantities obtained in the experiment (listed in columns 3 and 4 in Tab. 1). For example, the theoretically calculated energy difference between neutral Rh and its corresponding anion $Rh^-$ was found to be 1.2 eV, which is in agreement with the first peak in the $Rh^-$ experimental PES spectra at 1.2 eV as can be seen in the top graph in Figure 1. Nevertheless, as the cluster size increases, several factors need to be taken into consideration when calculating these energies for them to match the experimental data. For example, the ground state structures of the anion and its corresponding neutral may differ. This fact leads to a broad peak in the spectrum, complicating the interpretation of the PES peak assignments. Another issue to be considered is the presence of several low lying structural isomers and spin multiplicities close in energy at each cluster size. Therefore the calculations were performed for a number of possible structures for both the anionic and neutral $Rh_n$ clusters (for $n = 1-9$). The lowest energy isomers for the neutral case together with their spin multiplicity for $n = 2-9$ are shown in Figure 2. The same information for the anions are shown in Figure 3. Depending on the experimental conditions, more than one isomer and/or spin state can be produced in the beam. Therefore, for a synergistic interpretation of the PES spectra, the calculations must include all allowed spin states and all possible isomeric forms for both the neutral and the anionic configurations. As will be discussed further, if the calculated energies agree with experimental data, one can claim that the ground state geometry and its multiplicity has been identified.

Ground state structures and spin states of $Rh_n$ clusters have been a subject of controversy over the the past years as already mentioned. With such widely varying results, it was imperative to combine computational results with experimental data to elucidate this issue. For $Rh_3^-$ we found an isosceles triangle with multiplicity $M = 5$ to be the ground state. An equilateral triangle was, in fact, found to be structurally unstable. Neutral $Rh_3$ also has an isosceles triangle structure with multiplicity $M = 6$. In this case our B3LYP results do not agree with the previous theoretical results in references [12,13,22]. These found $Rh_3$ to have an equilateral triangle ground state structure with $M = 4$. Our calculated ADE of 1.16 eV and VDE of 1.27 eV for the $Rh_3$ in the isosceles triangle structure are in good agreement with the experimental ADE of 1.0 eV and VDE of 1.2 eV.

For $Rh_4$, many different geometries, ranging from squares to triangular pyramids [12,13,17], were proposed as the ground state structure. In this work, we found a bent rhombus structure as the global minimum as in reference [17], but with a multiplicity $M = 7$ (structure (a) in Fig. 2). We find a distorted tetrahedron to be higher in energy by 0.02 eV (structure (b) in Fig. 2). The anion ground state has a multiplicity $M = 8$. The electronic ground

**Table 1.** Experimental and calculated ADE and VDE of various clusters studied in this work. All energies are in eV. The superindex $a$ and $b$ refer to isomers a and b shown in Figures 2 and 3.

| Cluster | Structure | Experimental | | Calculated | |
|---|---|---|---|---|---|
| | | ADE | VDE | ADE | VDE |
| Rh | | – | 1.10 | – | 1.20 |
| $Rh_2$ | Dimer | 1.50 | 1.65 | 1.64 | 1.65 |
| $Rh_3$ | Isosceles triangle | 1.0 | 1.2 | 1.16 | 1.27 |
| $Rh_4$ | Bent rhombus$^a$ | 0.7 | 0.9 | 1.02 | 1.12 |
| $Rh_5$ | Triangular bi-pyramid$^a$ | 1.4 | 1.47 | 1.32$^a$ | 1.59$^a$ |
| $Rh_5$ | Square pyramid$^b$ | 1.4 | 1.47 | 1.40$^b$ | 1.51$^b$ |
| $Rh_6$ | Octahedron | 1.4 | 1.5 | 1.44 | 1.46 |
| $Rh_7$ | Pentagonal bi-pyramid$^a$ | 2.1 | 2.2 | 2.33$^a$ | 2.74$^a$ |
| $Rh_7$ | Capped-prism$^b$ | 2.1 | 2.2 | 2.07$^b$ | 2.10$^b$ |
| $Rh_8$ | Bi-capped octahedron$^a$ | 2.1 | 2.3 | 2.17$^a$ | 2.20$^a$ |
| $Rh_8$ | Capped prism$^b$ | 2.1 | 2.3 | 2.11$^b$ | 2.13$^b$ |
| $Rh_9$ | Capped anti-prism | 2.2 | 2.4 | 2.41 | 2.42 |

**Table 2.** Structure, electronic state, calculated binding energies ($E_b$) per atom, spin multiplicity, HOMO-LUMO gaps, and symmetry group associated to $Rh_n$ ($n = 2-9$) clusters. The superindex $a$ or $b$ refers to isomers shown in Figures 2 and 3.

| $Rh_n$ | Structure | State | | $E_b$/atom (eV) | $2S+1$ | | H-L (eV) | | Symmetry | |
|---|---|---|---|---|---|---|---|---|---|---|
| | | Neutral | Anion | Neutral | Neutral | Anion | Neutral | Anion | Neutral | Anion |
| $Rh_2$ | Dimer | *und.* | $4\Sigma_g$ | 0.8 | 5 | 4 | 1.38 | 1.34 | $D_{\infty h}$ | $D_{\infty h}$ |
| $Rh_3$ | Isosceles triangle | $6A_2$ | $5A_1$ | 1.38 | 6 | 5 | 2.26 | 1.42 | $C_{2v}$ | $C_{2v}$ |
| $Rh_4$ | Bent rhombus$^a$ | 7A | 8A | 1.72 | 7 | 8 | 2.15 | 0.91 | $C_1$ | $C_1$ |
| $Rh_4$ | Tetrahedron$^b$ | *und* | 6A | 1.72 | 7 | 6 | 2.59 | 1.01 | $T_d$ | $C_1$ |
| $Rh_5$ | Triangular bi-pyramid$^a$ | $8B_1$ | $9A_2$ | 1.82 | 8 | 9 | 1.30 | 1.36 | $C_{2v}$ | $C_{2v}$ |
| $Rh_5$ | Square pyramid$^b$ | *und.* | *und.* | 1.85 | 6 | 7 | 1.81 | 1.10 | $C_{4v}$ | $C_{4v}$ |
| $Rh_6$ | Octahedron | *und.* | $8A_u$ | 2.05 | 7 | 8 | 1.67 | 0.78 | $O_h$ | $S_2$ |
| $Rh_7$ | Pentagonal bi-pyramid$^a$ | 14A | 13A′ | 2.13 | 14 | 13 | 1.51 | 1.49 | $C_1$ | $C_S$ |
| $Rh_7$ | Capped-prism$^b$ | 12A′ | 13A′ | 2.09 | 12 | 13 | 1.04 | 0.99 | $C_S$ | $C_S$ |
| $Rh_8$ | Bi-capped octahedron$^a$ | $13A_1$ | 14A | 2.24 | 13 | 14 | 1.40 | 0.84 | $C_{2v}$ | $C_1$ |
| $Rh_8$ | Capped prism$^b$ | 13A | 14A | 2.21 | 13 | 14 | 1.11 | 1.84 | $C_1$ | $C_1$ |
| $Rh_9$ | Capped anti-prism | 18A | 17A | 2.39 | 18 | 17 | 1.47 | 1.74 | $C_1$ | $C_1$ |

state is A, and its binding energy is 1.72 eV (see Tab. 2 column 3). Our calculated ADE = 1.0 and VDE = 1.1 eV for the ground state match more closely the second threshold and peak at 1.0 eV and 1.2 eV respectively in the experimental PES of $Rh_4^-$ (Fig. 1). However, we have not been able to identify a structure or spin state that can explain the first peak at 0.8 eV in the PES. We only speculate that this could be due to a transition from the spin-excited state of the anion to a neutral state since the $M = 6$ of the anion is only 0.03 eV higher than the $M = 8$ state with an electronic ground state A. It is interesting to note that a regular tetrahedron isomer has a singlet as the lowest energy state for the neutral cluster. Reference [12] claimed this to be the ground state of $Rh_4$, but we find this isomer 0.27 eV higher than the bent rhombus with a multiplicity $M = 7$.

For the neutral $Rh_5$ cluster, we find that a triangular bi-pyramid structure with a multiplicity $M = 8$ and electronic state $B_1$ is the ground state (structure (a) in Fig. 2). A square pyramid with $M = 6$ is only 0.06 eV higher in energy (structure (b) in Fig. 2). This in general agrees with most of the published results in the literature [12,18–21,23]. For the anion, the square pyramid with $M = 7$ is 0.12 eV lower than the triangular bi-pyramid, in agreement with the results reported in reference [13]. Nevertheless, it is interesting that the square pyramid structure with multiplicity $M = 8$ is only 0.08 eV higher in energy than the same structure with multiplicity $M = 6$. Earlier calculations have also found a square pyramid structure to be the ground state of the neutral, with multiplicities $M = 6$ and $M = 8$ to be nearly degenerate [12,23]. Our calculated ADE is 1.4 eV and VDE is 1.47 eV for the square pyramid, and for the triangular bi-pyramid we found an ADE of 1.32 eV and a VDE of 1.59 eV. Both the quantities are in reasonable agreement with the experimental results as can be seen in Table 1.

For $Rh_6$ we find an octahedron with $M = 7$ (shown in Fig. 2) to be the ground state. The ground state anion is also an octahedron with $M = 8$ (shown in Fig. 3). However, earlier calculations [18,19] had found a singlet octahedron to be the ground state for $Rh_6$. Another result is a prism structure with $M = 7$ which has been found as global minima in reference [17]. FIR-MPD experimental study combined with DFT in reference [30]

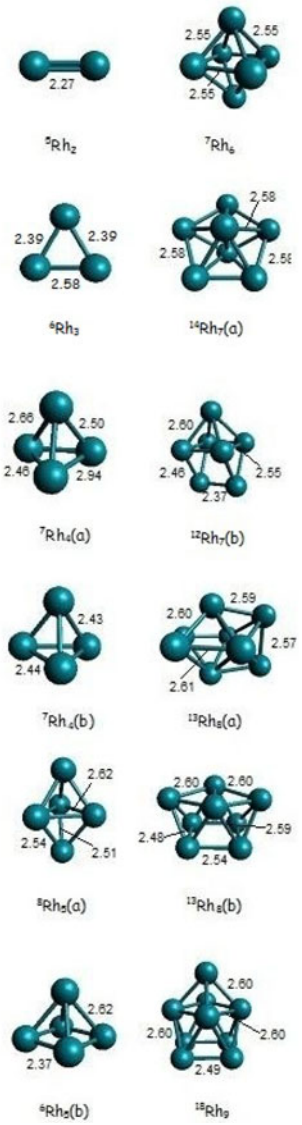


**Fig. 2.** Calculated structures of neutral $Rh_n$ clusters and its multiplicities: $Rh_4$(a) and $Rh_4$(b) are a bent rhombus and a tetrahedron respectively. $Rh_5$(a) and $Rh_5$(b) are the triangular bi-pyramid and square pyramid respectively. $Rh_6$ is an octahedron. $Rh_7$(a) and $Rh_7$(b) are a pentagonal bi-pyramid and a capped prism, respectively. $Rh_8$(a) and $Rh_8$(b) bicapped octahedron and capped prism, respectively. $Rh_9$ is a capped square anti-prism. For all cases, bond lengths are shown in Angstroms.

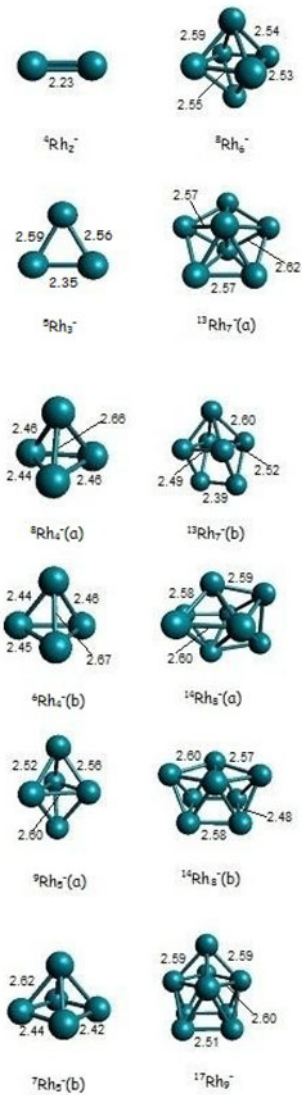


**Fig. 3.** Calculated structures of $Rh_n$ cluster anions and its multiplicities: $Rh_4$(a) and $Rh_4$(b) a bent rhombus and a tetrahedron, respectively. $Rh_5$(a) and $Rh_5$(b) a triangular bi-pyramid and a square pyramid, respectively. $Rh_6$ is an octahedron. $Rh_7$(a) and $Rh_7$(b) are a pentagonal bi-pyramid, a capped prism, respectively. $Rh_8$(a) and $Rh_8$(b) are the bi-capped octahedron and capped prism, respectively. $Rh_9$ is a bi-capped square anti-prism. In all cases, bond lengths are shown in Amstrongs.

also found an octahedral structure as the ground state for the $Rh_6^+$ cluster. DFT calculations in this work assigned to this structure a multiplicity $M = 10$. The corresponding anion is to be expected to differ in multiplicity from the neutral cluster by 1 as a single electron is removed. In that spirit, our results match the exact same geometry and, therefore, the same FIR spectra when we considered the cationic $Rh_6^+$ cluster, but we found a different ground state multiplicity of $M = 8$. This difference is due to the use of a different exchange-correlation functional. We use B3LYP that incorporates 20% Hartree-Fock (HF) exchange. Harding et al. [30] used the PBE1 exchange and correlation functional that includes 25% HF exchange. We believe that our results for the anion and the neutral cluster, when combined with the FIR-MPD DFT study [30], provides a good understanding for this cluster for all charge states. More interestingly, the present study points out the limits to which we can predict their spin states within the hybrid + DFT exchange-correlation functional framework.

For $Rh_7$, we found a pentagonal bi-pyramid with multiplicity $M = 14$ and electronic state A (shown in structure (a) in Fig. 2) to be the ground state. This result is in very good agreement with earlier calculations [13] and it also is in agreement with the results in

references [18,19,30]. However, this result is in disagreement with [17] which claims a capped prism with multiplicity $M = 12$ to be the ground state. The calculated ADE of 2.334 eV and VDE of 2.74 eV for our ground state pentagonal bi-pyramid do not match the experimental results very well. Interestingly, we found that the capped prism structure with multiplicity $M = 12$ and electronic state A' reported in reference [17] is higher in energy by only 0.2 eV (structure (b) in Fig. 2). The calculated VDE of 2.1 eV and ADE of 2.07 eV for this match more closely the experimental data, and these results are reported in Table 1. This observation suggests that this slightly higher energy isomer could have been produced in the experiments in greater abundance due to kinetic reasons. Finally, it is interesting to note that in the FIR-MPD combined with DFT study [30] for the cationic $Rh_7^+$ cluster, the pentagonal bi-pyramid is found as the ground state with $M = 11$. This again coincides with our ground state geometry for the neutral $Rh_7$ isomer, supporting our findings. Furthermore the infra red spectra of the cationic $Rh_7^+$ has been calculated matching with precision the experimental FIR-MPD in reference [30]. Despite the agreement in geometry, the lowest spin configuration differs from what our results predict. The possible source of this discrepancy is the Hartree-Fock exchange weight content as discussed in earlier paragraphs.

For $Rh_8$ the ground state geometry is a bicapped octahedron structure with $M = 13$ and electronic state $A_1$ (structure (a) in Fig. 2), in agreement with the bicapped octahedron cationic cluster obtained in references [29,30]. But the multiplicity of the cationic $Rh_8^+$ cluster reported as $M = 12$ does not match our result. Earlier results [17] had obtained a cube with multiplicity $M = 13$ as the ground state for the neutral cluster. However, we found the cube 0.61 eV higher in energy. Our results also show a capped prism (structure (b) in Fig. 2) with multiplicity $M = 13$ for the neutral cluster that is 0.22 eV higher in energy than the ground state. The ground state ADE of 2.17 eV is in excellent agreement with the experimental value of 2.1 eV as shown in Table 1. We believe that this study together with the FIR-MPD and DFT study reported in reference [29] for $Rh_8^+$ provides a sound and complete picture for the geometry and electronic structure for this cluster case.

For $Rh_9^-$ we obtained a capped square anti-prism structure (or trigonal capped prism) with multiplicity $M = 17$ and electronic state A as the ground state. The neutral is also a capped square anti-prism with multiplicity $M = 18$. These results reproduce the experimental IR spectra in reference [30] when the cationic cluster was calculated with multiplicity $M = 15$. The previously reported capped cube with multiplicity $M = 12$ was found to be higher (1.24 eV) in energy for the neutral species $Rh_9$. In fact, we found the capped cube structure to be unstable. Our calculated VDE of 2.42 eV for the capped anti-prism structure matches the experimental PES results almost exactly. We find the calculated ADE to be 2.41 eV.

Finally, our results for the electronic state, calculated binding energies ($E_b$) and the spin state are shown in Table 2. In this table, column 1 indicates the cluster size, column 2 indicates the ground state geometry, columns 3 and 4 show the electronic state, column 5 shows the calculated values for the binding energy per atom, $E_b$, defined as

$$E_b = [nE_{Rh} - E_T(\mathrm{Rh}_n)]/n, \quad (1)$$

where $n$ is the number of atoms, $E_{Rh}$ is the energy of a rhodium atom and $E_T(\mathrm{Rh}_n)$ is the total energy of the $n$ atom cluster. In columns 6 and 7 the corresponding multiplicity for the neutral and anionic cluster in their ground state geometries are shown. Columns 8 and 9 show the gap between the highest occupied and the lowest unoccupied molecular orbitals, known as the HOMO-LUMO gap. Finally, in columns 10 and 11, we show the group symmetry for both, neutrals and anions. The binding energy and HOMO-LUMO gaps are indicators of relative stability. In fact, simple metal clusters show large gaps at magic numbers. We find that the $E_b$ per atom steadily increases over the size range of $n = 1{-}9$. The HOMO-LUMO gap has large values for $n = 3{-}4$, but then decreases with size. An important outcome of the present study is that, in all the cases studied, the best agreement between experimental and calculated spectra was found for the geometry corresponding to the putative global minimum. However, agreement was not found in the lowest energy spin multiplicity between the calculated ones in reference [30] and the present work, despite the fact that both theoretical DFT approaches use Gaussian03 package and both use hybrid functionals. On the other hand, the IR spectra has been reproduced correctly for each size compared giving indications that the geometries are the correct ones. Thus, the discrepancy is possibly due to the difference in the fractions of HF exchange that the B3LYP and PBE1 functionals use. Therefore, it is important to notice that despite the achieved agreement in the geometry for both cations and anions between theory and experiment, obtained by means of such hybrid functionals, it is clear that a reliable description of the spin multiplicity and electronic structure for these highly open shell systems remains a challenge.

## 5 Summary

In the present work, we have performed a comprehensive study of the electronic, magnetic and structural properties of both anionic and neutral, $(\mathrm{Rh}_n)^-$ and $\mathrm{Rh}_n$ for $(n = 1{-}9)$, clusters by using a synergistic approach which combined anion photoelectron spectroscopy and DFT theoretical calculations. The total energy calculations account for the photo detachment spectra with reasonable accuracy and suggest that the ground state structures of these clusters have been identified in our calculations. The ground state geometries here obtained are also in excellent agreement with those obtained by means of the combined far-infrared multiple photon dissociation spectroscopy and density functional theory study for cationic $(\mathrm{Rh}_n)^+$ clusters in reference [30]. However, one should keep in mind that given the finite resolution of the experiments, and

limitations of the approximation made for the exchange-correlation functionals, there is always a degree of uncertainty involved in identifying the ground state structures. Within the limitations, we believe our study along with those in reference [30] produce the most reliable information so far. In this combined theoretical-experimental work we demonstrate the reliability of hybrid exchange-correlation functionals in identifying the correct ground sate geometry of these clusters. Some small differences in the spin manifold have been observed though, when comparing the calculations in reference [30] at the same ground state geometries with our calculations. This is due to the difference in the weighting of the H-F exchange functional. It is clear that a more decisive EPR type experiment is required to appropriately determine the factors underpinning the performance of the hybrid functional for 4*d* transition metals in general. Adiabatic detachment energies, vertical detachment energies, binding energies, magnetic moments as well as the HOMO-LUMO gaps have been calculated. The stability and dependence of these properties on the cluster sizes has been analyzed. Most interestingly, these results have shown that small rhodium clusters are magnetic and that some of them even have quite large magnetic moments. If one extrapolates, this result correlates well with earlier Stern-Gerlach experiments [6,15] in bigger size clusters. Work to extend such studies to larger cluster sizes is also in progress.

M.R.B. and F.B.Z. acknowledge support from PAPIIT IN110112, UNAM project, and from DGSCA UNAM. Some calculations were performed at the the suprcomputer Kan-Balam at the supercomputer center in UNAM while others have been done at the computing facility at HRI (http://www.cluster.hri.res.in). F.B.Z. acknowledges support from CONACYT (financial support No. 227089), and to the IIM (Instituto de Investigaciones en Materiales) for the use of its facilities. This material (KHBs experimental contribution) is based on work supported by the Division of Materials Sciences and Engineering, Office of Basic Energy Sciences, US Department of Energy under Grant No. DE-FG02-09ER46558.

## References

1. I.M.L. Billas, A. Chatelain, W.A. de Heer, Science **265**, 1682 (1994)
2. J.P. Bucher, D.C. Douglass, L.A. Bloomfiled, Phys. Rev. Lett. **66**, 3052 (1991)
3. S.E. Apsel, J.W. Emmert, J. Deng, L.A. Bloomfield, Phys. Rev. Lett. **76**, 1441 (1996)
4. E.K. Parks, S.J. Riley, Z. Phys. D **33**, 59 (1995)
5. E.K. Parks, L. Zhu, J. Ho, S.J. Riley, J. Chem. Phys. **102**, 7377 (1995)
6. E.K. Parks, L. Zhu, J. Ho, S.J. Riley, J. Chem. Phys. **100**, 7206 (1994)
7. O. Sipr, M. Kosuth, H. Ebert, Phys. Rev. B **70**, 174423 (2004)
8. M.L. Tiago, Y. Zhou, M.M.G. Alemany, Y. Saad, J.R. Chelikowsky, Phys. Rev. Lett. **97**, 147201 (2006)
9. R. Felix-Medina, J. Dorantes-Davila, G.M. Pastor, Phys. Rev. B **67**, 094430 (2003)
10. K.W. Edmonds, C. Binns, S.H. Baker, S.C. Thornton, C. Norris, J.B. Goedkoop, M. Finazzi, N.B. Brookes, Phys. Rev. **60**, 472 (1999)
11. B.V. Reddy, S.N. Khanna, B.I. Dunlap, Phys. Rev. Lett. **70**, 3323 (1993)
12. B.V. Reddy, S.K. Nayak, S.N. Khanna, B.K. Rao, P. Jena, Phys. Rev. B **59**, 5214 (1999)
13. T. Futschek, M. Marsman, J. Hafner, J. Phys. Condens. Matter **17**, 5927 (2005)
14. D. Majundar, K. Balasubramanian, J. Chem. Phys. **106**, 4055 (1997)
15. A.J. Cox, J.G. Louderback, L.A. Bloomfield, Phys. Rev. Lett. **71**, 923 (1993)
16. A.J. Cox, J.G. Louderback, S.E. Apsel, L.A. Bloomfield, Phys. Rev. B **49**, 12295 (1994)
17. Y.-C. Bae, H. Osanai, V. Kumar, Y. Kawazoe, Phys. Rev. B **70**, 195413 (2004)
18. Y. Jinlong, F. Toigo, W. Klein, Phys. Rev. B **50**, 7915 (1994)
19. Y. Jinlong, X. Chuanyun, X. Shangda, W. Klein, Phys. Rev. B **48**, 8253 (1993)
20. K.K. Das, K. Balasubramanian, J. Chem. Phys. **93**, 625 (1990)
21. D. Dai, K. Balasubramanian, Chem. Phys. Lett. **195**, 207 (1992)
22. S.K. Nayak, S.E. Weber, P. Jena, K. Wildberger, R. Zeller, P.H. Dederichs, V.S. Stepanyk, W. Hergert, Phys. Rev. B **56**, 8849 (1997)
23. P. Ghosh, R. Pushpa, S. de Gironcoli, S. Narasimhan, J. Chem. Phys. **128**, 194708 (2008)
24. S.M. Hamilton, W.S. Hopkins, D.J. Harding, T.R. Walsh, P. Gruene, M. Haertelt, A. Fielicke, G. Meijer, S. Mackenzie, J. Am. Chem. Soc. **132**, 1448 (2010)
25. S.M. Hamilton, W.S. Hopkins, D.J. Harding, T.R. Walsh, M. Haertelt, C. Kerpal, P. Gruene, G. Meijer, A. Fielicke, S. Mackenzie, J. Phys. Chem. A **115**, 2489 (2011)
26. A. Fielicke, G. von Helden, G. Meijer, D.B. Pedersen, B. Simard, D.M. Rayner, J. Phys. Chem. B **108**, 14591 (2004)
27. X. Li, A. Grubisic, S.T. Stokes, J. Cordes, G.F. Gantefoer, K.H. Bowen, B. Kiran, M. Willis, P. Jena, R. Burgert, H. Schnoeckel, Science **315**, 356 (2007)
28. H. Wang, Y.J. Ko, L.G. García, P. Sen, M.R. Beltrán, K.H. Bowen, Phys. Chem. Chem. Phys. **13**, 7685 (2011)
29. D.J. Harding, T.R. Walsh, S.M. Hamilton, W.S. Hopkins, S.R. Mackenzie, P. Gruene, M. Haertelt, G. Meijer, A. Fielicke, J. Chem. Phys. **132**, 011101 (2010)
30. D.J. Harding, P. Gruene, M. Haertelt, G. Meijer, A. Fielicke, S.M. Hamilton, W.S. Hopkins, S.R. Mackenzie, S.P. Neville, T.R. Walsh, J. Chem. Phys. **133**, 214304 (2010)
31. M. Gerhards, O.C. Thomas, J.M. Nilles, W.J. Zheng, K.H. Bowen, J. Chem. Phys. **116**, 10247 (2002)
32. D.G. Leopold, J. Ho, W.C. Lineberger, J. Chem. Phys. **86**, 1715 (1987)
33. A. Bergner, M. Dolg, W. Küchle, H. Stoll, H. Preuss, Mol. Phys. **80**, 1431 (1993)
34. J.H. Wood, A.M. Boring, Phys. Rev. B **18**, 2701 (1978)
35. D. Andrae, U. Haeussermann, M. Dolg, H. Stoll, H. Preuss, Theor. Chim. Acta **77**, 123 (1990)
36. Institute for Theoretical Chemistry, http://www.theochem.uni-stuttgart.de/pseudopotentials/index.en.html

37. P.J. Stephens, F.J. Devlin, C.F. Chabalowski, M.J. Frisch, J. Phys. Chem. **98**, 11623 (1994)
38. K.A. Gingerich, D.L. Cocke, J. Chem. Soc. Chem. Commun. **1**, 536 (1972)
39. M.J. Frisch, G.W. Trucks, H.B. Schlegel, G.E. Scuseria, M.A. Robb, J.R. Cheeseman, J.A. Montgomery Jr., T. Vreven, K.N. Kudin, J.C. Burant, J.M. Millam, S.S. Iyengar, J. Tomasi, V. Barone, B. Mennucci, M. Cossi, G. Scalmani, N. Rega, G.A. Petersson, H. Nakatsuji, M. Hada, M. Ehara, K. Toyota, R. Fukuda, J. Hasegawa, M. Ishida, T. Nakajima, Y. Honda, O. Kitao, H. Nakai, M. Klene, X. Li, J.E. Knox, H.P. Hratchian, J.B. Cross, V. Bakken, C. Adamo, J. Jaramillo, R. Gomperts, R.E. Stratmann, O. Yazyev, A.J. Austin, R. Cammi, C. Pomelli, J.W. Ochterski, P.Y. Ayala, K. Morokuma, G.A. Voth, P. Salvador, J.J. Dannenberg, V.G. Zakrzewski, S. Dapprich, A.D. Daniels, M.C. Strain, O. Farkas, D.K. Malick, A.D. Rabuck, K. Raghavachari, J.B. Foresman, J.V. Ortiz, Q. Cui, A.G. Baboul, S. Clifford, J. Cioslowski, B.B. Stefanov, G. Liu, A. Liashenko, P. Piskorz, I. Komaromi, R.L. Martin, D.J. Fox, T. Keith, M.A. Al-Laham, C.Y. Peng, A. Nanayakkara, M. Challacombe, P.M.W. Gill, B. Johnson, W. Chen, M.W. Wong, C. Gonzalez, J.A. Pople, *Gaussian 03*, Revision D.1 (Gaussian, Inc., Wallingford, 2005)